



Q spoiling in deformed optical microdisks due to resonance-assisted tunneling

Julius Kullig and Jan Wiersig

Institut für Theoretische Physik, Otto-von-Guericke-Universität Magdeburg, Postfach 4120, D-39016 Magdeburg, Germany

(Received 30 May 2016; published 2 August 2016)

A recent experiment by Kwak *et al.* [[Sci. Rep. 5, 9010 \(2015\)](#)] demonstrated the relevance of resonance-assisted tunneling for optical microcavities where resonance chains emerge in phase space due to boundary deformations. In this paper we adapt the perturbative description of resonance-assisted tunneling to calculate optical modes and the imaginary part of their complex wavenumber which determines the lifetime of the mode. We demonstrate our method at three example cavity shapes and compare our results to numerical data and perturbation theory for weakly deformed microdisk cavities.

DOI: [10.1103/PhysRevE.94.022202](https://doi.org/10.1103/PhysRevE.94.022202)

I. INTRODUCTION

Depending on their boundary shape, optical microdisk cavities show various kinds of ray dynamics ranging from integrable in a circular cavity to fully chaotic, e.g., in a cardioid. However, generic deformations exhibit mixed dynamics where regions of regular and chaotic dynamics coexists in phase space [1,2]. This mixed phase space is typically interspersed by resonance chains which emerge due to the Poincaré-Birkhoff theorem from perturbed periodic orbits [3,4]. These resonance chains consists of an alternating sequence of stable and unstable periodic orbits surrounded by a separatrix with a chaotic layer, see Fig. 1(d) for an example. Classically disjoint regions in phase space are in general coupled quantum mechanically by dynamical tunneling [5,6].

Therefore, optical microcavities are paradigmatic systems to study dynamical tunneling [7,8]. Here, the quasi-two-dimensional dynamics of either the electric or magnetic field is described by a Schrödinger-type mode equation [9]. Therefore, dynamical tunneling leads to a finite Q factor (or lifetime) of optical modes, even in systems where rays are trapped for arbitrarily long times due to total internal reflection. On the other hand, the coupling of classically separated regions via dynamical tunneling allows, e.g., the pumping of high- Q modes [10,11] or the creation of tunneling-induced transparency [12].

However, classical phase-space perturbations, e.g., generated by boundary deformations of the cavity, have a strong impact on dynamical tunneling and typically further reduce the lifetime of optical modes in comparison to a circular cavity. This Q spoiling has been traced back for strong perturbations to chaos-assisted tunneling [13–16], where regions of chaotic ray dynamics in phase space enhance dynamical tunneling.

But also for relatively weak perturbations Q spoiling is observed [17]. In this regime of weak perturbations, nonlinear resonance chains in the phase space can enhance dynamical tunneling, which is then called resonance-assisted tunneling (RAT). RAT is well investigated theoretically for kicked Hamiltonian systems (two-dimensional maps) [18–23] and experimentally verified in microwave resonators [24]. Its application to optical microcavities is less investigated. But here a recent experiment by Kwak *et al.* [25] pointed out a particular relevance: They observe an avoided resonance crossing in the real part of complex wave number kR and verified that the coupling strength between optical modes

is connected to the area surrounded by the separatrix of a resonance chain in phase space.

In this paper, we demonstrate that RAT has also an impact on the lifetime of modes in a deformed microcavity which is determined by the imaginary part of the complex wave number kR . For this purpose, we model one dominant resonance chain in phase space by a generalized pendulum approximation from which we perturbatively deduce the coupling between modes of the circular cavity. Thereby, we predict the imaginary part of the complex wave numbers and the mode pattern of the microcavity.

The paper is organized as follows. In Sec. II we introduce the systems which we investigate throughout the article and describe ray and wave dynamics in a deformed optical microcavity. In Sec. III we explain the derivation of complex wave numbers and optical mode pattern from the generalized pendulum approximation of the resonance chain in phase space and we present a comparison of our results to an existing perturbation theory for weakly deformed microcavities [26]. A conclusion and outlook is given in Sec. IV.

II. DEFORMED OPTICAL MICROCAVITIES

In this section we first discuss the ray dynamics of deformed optical microcavities in phase space (Sec. II A). Second, we describe the wave dynamics by the mode equation (Sec. II B). More details on ray and wave dynamics can be found in Ref. [27]. Furthermore, we introduce the systems on which we focus in this paper.

A. Ray dynamics

Rays inside microcavities with homogeneous refractive index n propagate on straight lines until boundary reflections. Therefore it is convenient to describe the ray dynamics in a Poincaré section where positions q along the boundary and tangential momenta $p = \sin \chi$ of the reflections are tracked, see Fig. 1(a). Since we consider only cavities with mirror reflection symmetry, we restrict the phase space to positive momenta without loss of generality.

The ray dynamics in phase space shows nicely the characteristics of the boundary shape of the cavity. A perfect circular microdisk leads to integrable dynamics with action-angle variables (q, p) where p stays constant and q increases linearly under time evolution, see Fig. 1(b). For weak perturbations of

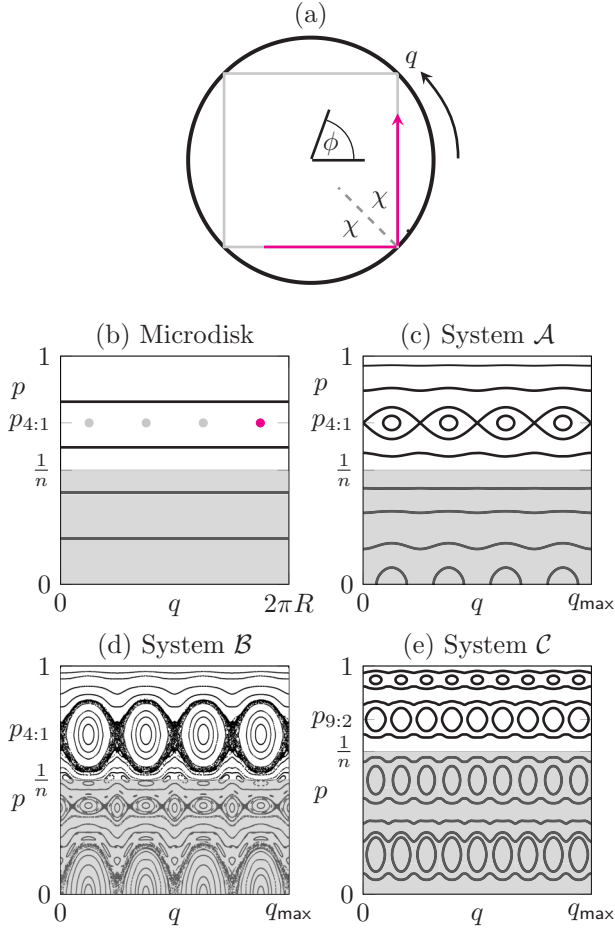


FIG. 1. A circular cavity with a periodic ray orbit is shown in (a); χ is the angle of incidence. Orbits (black curves with dots) are shown in the phase space $(q, p = \sin \chi)$ of (b) a circular cavity, (c) system \mathcal{A} , (d) system \mathcal{B} , and (e) system \mathcal{C} ; q_{\max} is the circumference of the deformed disk. Gray shaded regions indicate the leaky region.

the circular boundary the ray trajectories in phase space are deformed and resonance chains of order $r:s$ emerge around periodic orbits with momenta

$$p_{r:s} = \cos\left(\pi \frac{s}{r}\right) \quad (1)$$

and frequencies

$$\omega_{r:s} = 2\pi \frac{s}{r} \quad (2)$$

due to the Poincaré-Birkhoff theorem, see Fig. 1(c) for an example with $r:s = 4:1$. Here, s is the number of circumcircles after r reflections. In this paper we want to focus on the so-called microflower cavity [28–30] of the form

$$r(\phi) = R[1 + \epsilon \cos(N\phi)], \quad (3)$$

where a resonance chain can be easily create by adjusting (ϵ, N) . By increasing the perturbation strength ϵ further the chaotic layer of the separatrix is enlarged, see Fig. 1(d). Large resonance chains of higher order can be created by increasing N , see Fig. 1(e). In addition to the billiard dynamics, a leaky region is defined in phase space by the refractive index n .

TABLE I. The tabular shows the boundary parameters [see Eq. (3)] of the three systems which we consider in this paper. Furthermore, the refractive index and the order of the dominant resonance chain above the critical line is shown.

System	ϵ	N	n	$r:s$
\mathcal{A}	0.0025	4	2.0	4:1
\mathcal{B}	0.013	4	2.0	4:1
\mathcal{C}	0.002	9	1.6	9:2

Rays with $|p| < 1/n$ are not totally but partially reflected [31]. Therefore, resonance chains below the critical line are negligible for our purpose.

In the following, we want to have a dominant resonance chain above the critical line which we are able to model with a generalized pendulum approximation. Therefore, we set the parameters of the three systems on which we focus in the paper to the values listed in Table I. Note that also in systems \mathcal{A} [Fig. 1(c)] and \mathcal{C} [Fig. 1(e)] a thin chaotic layer around the separatrix exists, but it is too small to be visible in the plots.

B. Wave dynamics

Wave dynamics of optical microcavities is determined by Maxwell's equations which reduce for quasi-two-dimensional objects to the scalar mode equation

$$[\Delta + k^2 n^2(\vec{r})]\Psi(\vec{r}) = 0 \quad (4)$$

for Ψ representing the z direction of either the electric field (transverse magnetic [TM] polarization) or the magnetic field (transverse electric [TE] polarization) [9]. At the cavity's boundary Ψ and its normal derivative $\partial_\nu \Psi$ needs to be continuous with

$$\partial_\nu \Psi_{\text{in}} = \partial_\nu \Psi_{\text{out}} \quad \text{for TM polarization,} \quad (5)$$

$$\frac{1}{n_{\text{in}}^2} \partial_\nu \Psi_{\text{in}} = \frac{1}{n_{\text{out}}^2} \partial_\nu \Psi_{\text{out}} \quad \text{for TE polarization.} \quad (6)$$

Furthermore, the outgoing wave condition

$$\Psi(\rho, \phi) = h(k, \phi) \frac{\exp(ik\rho)}{\sqrt{\rho}} \quad (7)$$

for large ρ needs to be fulfilled. Consequently, Eq. (4) is solvable only for a discrete set of complex wave numbers $x = kR$. The real part of x determines the vacuum wavelength $\lambda = 2\pi R/\text{Re } x$ and the imaginary part of x describes the intensity loss of an optical mode in the microcavity in time as

$$\|\Psi(t)\|^2 = \int_{\text{cavity}} |\Psi|^2 d^2r = e^{-\Gamma t} \quad (8)$$

with loss rate $\Gamma = -2c \text{Im } x/R$. Therefore, the lifetime $\tau = 1/\Gamma$ of an optical mode is quantified by the quality factor $Q = -\text{Re } x/(2\text{Im } x)$. In the following we consider TM polarization. However, our methods are generalizable to TE polarization by using the appropriate values of x . In case of a circular microdisk, the complex wave numbers are computed

analytically as the roots of

$$S_m(x) = n \frac{J'_m(nx)}{J_m(nx)} - \frac{H'_m(x)}{H_m(x)} \quad (9)$$

with J and H being Bessel and Hankel functions both of the first kind. The resulting complex wave numbers $x_{m,l}$ and its corresponding optical modes $\Psi_{m,l}$ given by

$$\Psi_{m,l}(\rho, \phi; x) = \begin{cases} \frac{J_m(nk\rho)}{J_m(nx)} \cos(m\phi) & \text{for } \rho \leq R \\ \frac{H_m(k\rho)}{H_m(x)} \cos(m\phi) & \text{for } \rho > R \end{cases} \quad (10)$$

are labeled with two mode numbers representing the number of nodes in the azimuthal and radial directions, respectively.

Optical modes with small l are called whispering-gallery modes, indicating their characteristic to slide along the cavity's boundary. These modes typically have the highest lifetime for a certain range of $\text{Re } x$. In this paper we therefore focus on predicting complex wave numbers of these whispering-gallery modes. For an exact treatment of arbitrary deformed optical cavities, Eq. (4) needs to be solved numerically with, e.g., the boundary element method (BEM) [32]. In case of weakly deformed optical cavities with mirror reflection symmetry, a perturbative treatment of the deformation allows us to compute optical modes and complex wave numbers up to a minimal wavelength [26,33–36]. We compare our predictions of complex wave numbers based on RAT to the perturbation theory for optical cavities in Sec. III C. For a comparison of ray and wave dynamics we use a boundary Husimi representation [37] of an optical mode. For circular cavities the modes are concentrated around the momenta [31]

$$p_{m,l} = \frac{m}{n \text{Re } x_{m,l}} \quad (11)$$

with an exponential decay towards classically forbidden regions, see Fig. 2(a). Optical modes in weakly deformed cavities roughly mimic classical phase space structures as shown, e.g., for system \mathcal{A} in Figs. 2(b) and 2(d). Here, the long-lived modes avoid either the stable [Fig. 2(d)] or unstable [Fig. 2(b)] fixed point. Particular modes show a hybridization between two classically separated tori below and above a resonance chain, as shown in Fig. 2(c). Additional deviations between ray dynamics in a billiard system and waves in an optical cavity arise from the dielectric boundary conditions. The Goos-Hänchen shift $\Delta q \sim \lambda$ is the offset between the incoming and outgoing rays along q at the dielectric interface [38,39]. In Ref. [40] it was shown that the Goos-Hänchen shift lifts a periodic orbit in momentum due to the curved cavity shape. This periodic orbit shift (POS) together with Fresnel filtering [41,42] lead to wave mechanical corrections to the ray dynamics in p .

III. RESONANCE-ASSISTED TUNNELING FOR OPTICAL MICROCAVITIES

In this section we use a perturbative description of RAT to predict optical mode patterns and their loss rates. First, we use a generalized pendulum approximation to model one dominant resonance chain in phase space (Sec. III A). Afterwards, we deduce the mode coupling and the loss rates of optical modes from a perturbative treatment of the pendulum approximation

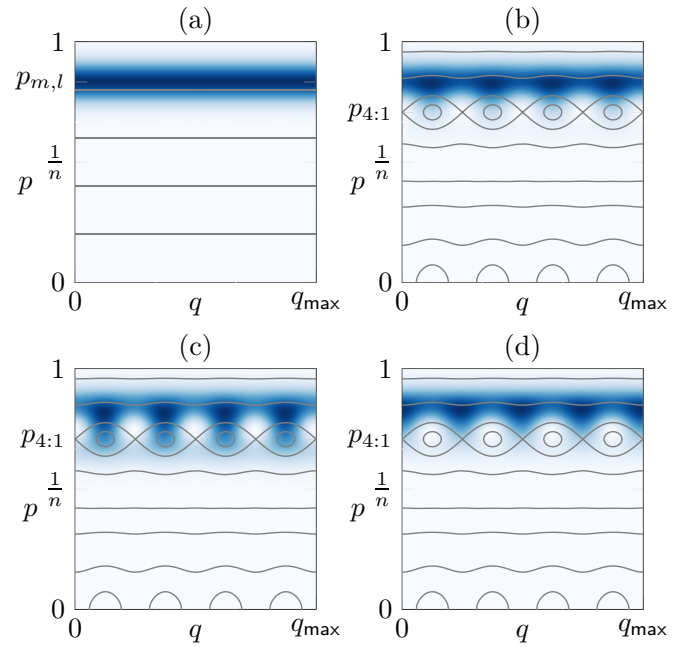


FIG. 2. Boundary Husimi function of optical modes in (a) a circular cavity and [(b)–(d)] system \mathcal{A} are shown from low intensity (white) to high intensity (dark blue). The mode numbers are [(a) and (b)] $(m,l) = (21,1)$, (c) $(m,l) = (22,1)$, and (d) $(m,l) = (23,1)$. Underlying classical phase-space structures are shown as gray curves.

(Sec. III B) and compare our results to the perturbation theory for deformed microdisk cavities (Sec. III C).

A. Generalized pendulum approximation

For the prediction of complex wave numbers we need to model one dominant resonance chain in phase space. Therefore, we use the so-called generalized pendulum approximation [6,18,43]

$$\mathcal{H}_{r;s}(q, p) = \mathcal{H}_0(p) + 2\mathcal{V}_{r;s} \cos\left(2\pi r \frac{q}{q_{\max}} + \phi_0\right), \quad (12)$$

which creates r resonance eyes in phase space between $q = 0$ and q_{\max} . The resonance chain is generated in phase space around the maximum of the dispersion $\mathcal{H}_0(p)$ which describes the integrable dynamics of the circular microdisk in the corotating frame with frequency $\omega_{r;s}$. This leads to a stationary resonance chain in $\mathcal{H}_{r;s}(q, p)$, meaning that an orbit inside the separatrix encircles one stable fixed point.

In Ref. [25] the quadratic approximation of $\mathcal{H}_0(p)$ was obtained via fitting the effective mass of the pendulum. In this paper we obtain a general dispersion $\mathcal{H}_0(p)$ for a circular cavity by exploiting the fact that Eqs. (1) and (2) hold for all rationals s/r and that the frequency function $\omega(p)$ is continuous. Therefore, we get

$$\omega(p) = 2 \arccos(p). \quad (13)$$

We define the Hamiltonian $\mathcal{H}_0(p)$ via integrating the corotating frequency function $\omega(p) - \omega_{r;s} = \partial \mathcal{H}_0 / \partial p$ as

$$\mathcal{H}_0(p) = \int_{p_{r;s}}^p [\omega(p') - \omega_{r;s}] dp', \quad (14)$$

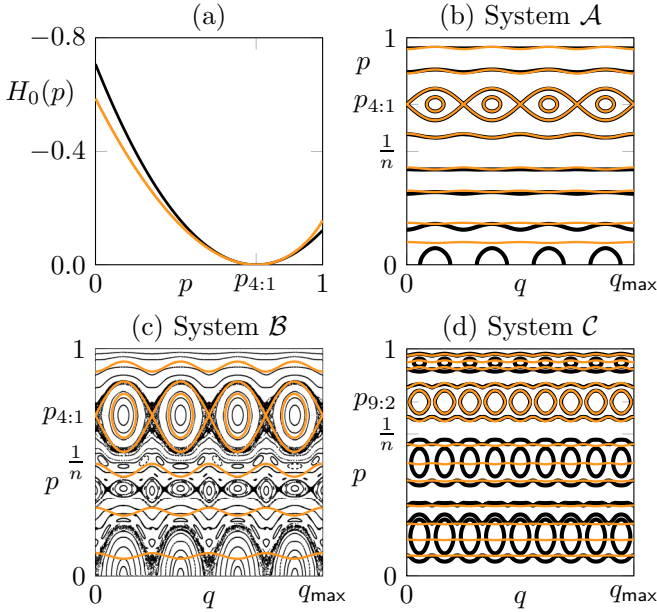


FIG. 3. Panel (a) shows the dispersion $\mathcal{H}_0(p)$ (light orange curve) given by Eq. (15) and its quadratic approximation (dark black curve), see Eq. (16). The panels (b)–(d) show the phase space (dark black curves with dots) of systems \mathcal{A} – \mathcal{C} , respectively. Orange curves are contours of the pendulum approximation $\mathcal{H}_{r:s}$.

which results in

$$\mathcal{H}_0(p) = 2 \left(p \arccos(p) - \sqrt{1-p^2} + \sqrt{1-p_{r:s}^2} \right) - \omega_{r:s} p. \quad (15)$$

The leading order of $\mathcal{H}_0(p)$ expanded around $p = p_{r:s}$ is the quadratic term

$$\mathcal{H}_0(p) = -\frac{(p - p_{r:s})^2}{\sqrt{1-p_{r:s}^2}} + \mathcal{O}[(p - p_{r:s})^3], \quad (16)$$

which nicely describes $\mathcal{H}_0(p)$ around $p_{r:s}$ as shown in Fig. 3(a). Note that the minus sign of \mathcal{H}_0 is not exceptional and appears, e.g., in approximations of resonance chains in the standard map, too (see, e.g., Ref. [43]). For system \mathcal{C} , the quadratic approximation of \mathcal{H}_0 is used, which gives slightly better results than the full $\mathcal{H}_0(p)$ in this case. An estimate of the perturbation strength $\mathcal{V}_{r:s}$ can be deduced from the linearized billiard dynamics of the stable periodic orbit of the resonance chain [21]; with the expansion of $\mathcal{H}_0(p)$ given by Eq. (16) this results in

$$\mathcal{V}_{r:s} = \left(\frac{q_{\max}}{2\pi R} \right)^2 \frac{\sqrt{1-p_{r:s}^2}}{4r^2} \left(\arccos \left[\frac{\text{Tr } J_{r:s}}{2} \right] \right)^2. \quad (17)$$

Here, $\text{Tr } J_{r:s}$ is the trace over the monodromy matrix of the stable periodic orbit. This estimate gives proper results for weak perturbations as in system \mathcal{A} and \mathcal{C} . However, for stronger perturbations as in system \mathcal{B} the linearized dynamics is insufficient to reproduce an accurate $\mathcal{V}_{r:s}$. In this case better results for $\mathcal{V}_{r:s}$ were achieved by numerically matching the area enclosed by the separatrix. For the three systems investigated in this paper the generalized pendulum approximations are compared to the ray dynamics in Figs. 3(b)–3(d). Note that the

regions where the ray dynamics is not well described by the pendulum approximation, e.g., near the bouncing ball orbit at $p = 0$, are inside the leaky region and therefore not important for our purpose.

B. Mode approximation

In this section we employ the above pendulum approximation of a resonance chain to predict the complex wave number $\tilde{x} = \tilde{k}R$ of an optical mode $\tilde{\Psi}$ in the deformed cavity from complex wave numbers $x = kR$ of optical modes Ψ in a circular cavity. Since we have to fulfill the *selection rules* of RAT [18,19,25], only modes with mode numbers associated to the order $r:s$ of the resonance chain contribute to the prediction. In case of optical microcavities, this means that a mode $(m, l = 1)$ can only couple to modes $(m - jr, l + js)$ with integer $j \geq 0$ [25]. Therefore, the linear combination we use to approximate the mode of the deformed cavity is

$$\tilde{\Psi}_{m,l}(\rho, \phi; \tilde{x}) = \mathcal{N}^{-1} \sum_{j \geq 0} a_j \Psi_{m-jr, l+js}(\rho, \phi; \tilde{x}), \quad (18)$$

with coefficients a_j which need to be determined and normalization constant $\mathcal{N}^2 = \sum_{j \geq 0} |a_j|^2$. From Eq. (8) we conclude that the imaginary part $\text{Im } \tilde{x}_{m,l}$ of complex wave numbers is in leading order proportional to $\|\tilde{\Psi}_{m,l}\|^2$. Therefore, our central assumption is

$$\text{Im } \tilde{x}_{m,l} = \mathcal{N}^{-2} \sum_{j \geq 0} |a_j|^2 \text{Im } x_{m-jr, l+js}. \quad (19)$$

The coefficients a_j are deduced from the generalized pendulum approximation $\mathcal{H}_{r:s}$ via secular perturbation theory, which results in a fixed $a_0 = 1$ and

$$a_j = \prod_{u \leq j} \frac{\mathcal{V}_{r:s} e^{i\phi_0}}{\mathcal{H}_0(p_{m,l}^{\text{mod}}) - \mathcal{H}_0(p_{m-ur, l+us}^{\text{mod}})} \quad (20)$$

for $j > 0$ [18,19]. For the three systems, $\phi_0 = \pi$ is the global phase from the Hamiltonian $\mathcal{H}_{r:s}$; see Eq. (12).

In contrast to the case of maps and billiard systems, optical modes satisfy dielectric boundary conditions on the cavity's interface while the generalized pendulum approximation $\mathcal{H}_{r:s}$ fits to the billiard dynamics of a closed system. In Ref. [25] the POS was respected by using augmented ray dynamics at fixed $\text{Re } x$. Here, we use a modified momenta $p_{m,l}^{\text{mod}}$ of an optical mode instead of $p_{m,l}$ given by Eq. (11). The advantage is that we can use the same generalized pendulum approximation for all modes, e.g., all values of $\text{Re } x$. The modified momenta are calculated from the Goos-Hänchen shift, which results in a periodic orbit shift given by [40]

$$\Delta p_{\text{POS}} = \frac{\Delta q(p_{r:s})}{2r_c} \sqrt{1-p_{r:s}^2} \quad (21)$$

with radius of curvature r_c . With an approximation for the Goos-Hänchen shift obtained by Artmann [39]

$$\Delta q(p) = \frac{2p}{\sqrt{n^2 p^2 - 1} \sqrt{1-p^2} \text{Re } k} \quad (22)$$

at $p = p_{r:s}$ and an average radius of curvature $r_c \approx R$ of stable and unstable periodic orbits along the $r:s$ resonance chain, this

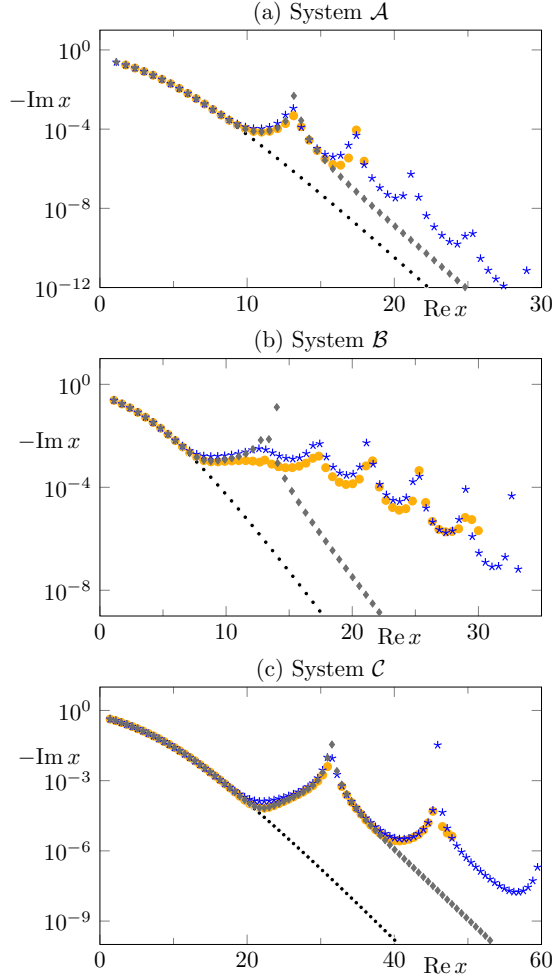


FIG. 4. Complex wave numbers for systems (a) \mathcal{A} , (b) \mathcal{B} , and (c) \mathcal{C} are shown in a semilogarithmic plot. Thick orange dots are numerically determined (BEM) and blue stars show the predicted values by Eq. (19). Gray diamonds represent the predictions based on the second-order perturbation theory from Ref. [26]. Small black dots correspond to complex wave numbers of a circular cavity.

leads to an effective shift,

$$\Delta m_{\text{POS}} = \frac{p_{r,s}}{\sqrt{p_{r,s}^2 - n^{-2}}}, \quad (23)$$

in the mode number m . Note that this shift in the mode number is around $\Delta m \sim 1.5$ (e.g., $\Delta m = 1.414214$ for system \mathcal{A}). Therefore, it cannot be seen as a small correction and has a considerable effect in Eq. (20). Since Fresnel-Filtering is typically small for large $\text{Re } x$ [42] we approximate $p_{m,l}^{\text{mod}}$ using POS only. Therefore, we get the modified momentum

$$p_{m,l}^{\text{mod}} = \frac{1}{n \text{Re } x_{m,l}} (m - \Delta m_{\text{POS}}). \quad (24)$$

Note that the effective shift in the mode number m is independent of m, l . Therefore, it is equal for all modes in the system.

For the three systems \mathcal{A} , \mathcal{B} , and \mathcal{C} , see Figs. 1(c)–1(e), the complex wave numbers predicted by Eq. (19) are shown in Fig. 4. They nicely correspond to numerically determined

values. Moreover, Eq. (19) is easy to use also for larger values of $\text{Re } x$ where $|\text{Im } x|$ is tiny so numerical methods have an enormous effort to determine its value. For this reason no further numerically determined values of x are shown in Fig. 4. We also analyzed modes with small $l > 1$ and get similar results.

With Eq. (18) the near field of an optical mode can be calculated. A comparison between the predicted and numerically determined mode pattern is shown in the upper panels of Fig. 5 for system \mathcal{A} . Modes with a small mode number are less influenced by the boundary deformation and look almost like optical modes of a circular cavity, see Fig. 5(a). Here, the energy gap [see Fig. 5(a) lower panel] of the involved modes is rather large so the coupling terms a_j in Eq. (20) are small. Right before and after the resonance peak, see Figs. 5(b) and 5(d), two involved modes are strongly coupled by a small energy denominator. They show a transition from localization on unstable periodic orbit [Fig. 5(b)] to localization on stable periodic orbit [Fig. 5(d)]. Note that such a transition has been also observed for maps [44,45] and for an optical mode with fixed mode numbers by changing system parameters [46]. The prediction by Eq. (18) fails very close to the resonance case, see Fig. 5(c), due to nearly vanishing energy denominators.

According to Eq. (18), we calculate the far-field amplitude $F_{m,l}(\phi)$ of a mode predicted by RAT via

$$F_{m,l}(\phi) \sim \sum_{j \geq 0} a_j \frac{e^{-i\pi(m-jr)/2}}{H_{m-jr}(\tilde{x}_{m,l})} \cos[(m-jr)\phi]. \quad (25)$$

In Fig. 6 the resulting far-field intensity pattern $|F_{m,l}(\phi)|^2$ for the mode $(m,l) = (21,1)$ in system \mathcal{A} is shown. For a comparison to numerically determined (BEM) far-field intensities, we normalized both pattern to the same value. Thus, a good agreement is observed.

C. Comparison to perturbation theory for weakly deformed microdisks

Next, we compare the RAT prediction of complex wave numbers to the perturbation theory for deformed microdisk cavities derived by Dubertrand *et al.* [26]. Here, the boundary deformation is treated as a perturbation to a circular cavity as

$$r(\phi) = R + \epsilon f(\phi). \quad (26)$$

The resulting complex wave numbers for TM modes with positive parity are in second-order perturbation theory given by [26]

$$\begin{aligned} \tilde{x}_{m,l} = x_{m,l} & \left[1 - \epsilon \mathcal{F}_{1,mm} + \epsilon^2 \left(\frac{1}{2} (3\mathcal{F}_{1,mm}^2 - \mathcal{F}_{2,mm}) \right. \right. \\ & + x_{m,l} (\mathcal{F}_{1,mm}^2 - \mathcal{F}_{2,mm}) \frac{H'_m(x_{m,l})}{H_m(x_{m,l})} \\ & \left. \left. - (n^2 - 1)x_{m,l} \sum_{p \neq m} \frac{\mathcal{F}_{1,mp} \mathcal{F}_{1,pm}}{S_k(x_{m,l})} \right) \right] \end{aligned} \quad (27)$$

with m and p non-negative and Fourier harmonics,

$$\mathcal{F}_{u,pm} = \frac{\epsilon_p}{\pi R^u} \int_0^\pi f(\phi)^u \cos(p\phi) \cos(m\phi) d\phi, \quad (28)$$

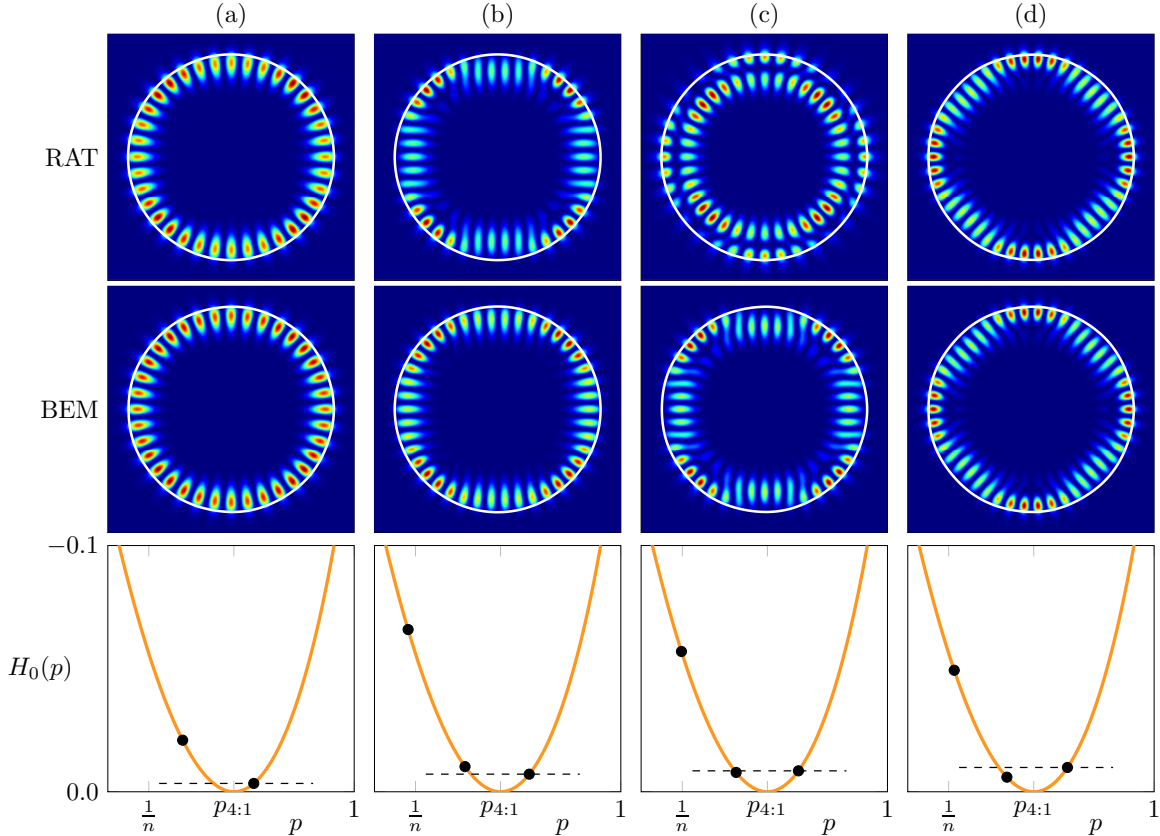


FIG. 5. The upper row shows the mode pattern predicted by RAT in Eq. (18) for system \mathcal{A} . In comparison, the middle panels shows the mode pattern numerically calculated with the BEM [32]. The dispersion relation given by \mathcal{H}_0 (curve), Eq. (15), is shown in the lower panels where thick dots at $[p_{m-jr,l+js}^{\text{mod}}, \mathcal{H}_0(p_{m-jr,l+js}^{\text{mod}})]$ illustrate the energy of involved modes with the modified momenta from Eq. (24). The dashed line is a guide to the eye. The mode numbers are (a) $(m, l) = (18, 1)$, (b) $(m, l) = (21, 1)$, (c) $(m, l) = (22, 1)$, and (d) $(m, l) = (23, 1)$.

of the boundary deformation function where ε_p is one for $p = 0$ and two otherwise. The comparison to the RAT predictions of x are shown in Fig. 4. Interestingly, the perturbation theory by Dubertrand *et al.* reproduces in first order no peak in $\text{Im } x$ (not shown). In second order only the first peak in $\text{Im } x$ is predicted. The reason is that modes with different azimuthal mode numbers are only coupled via the last term in Eq. (27) where

$\mathcal{F}_{1,pm}$ enters. In this paper we investigate deformation of the form $f(\phi) = R \cos(N\phi)$ [see Eq. (3)] where N corresponds to the number r of eyes in the dominant resonance chain. Therefore, the Fourier harmonics

$$\mathcal{F}_{1,pm} = \frac{\varepsilon_p}{4} (\delta_{m-p,\pm r} + \delta_{m+p,r}) \quad (29)$$

restrict the azimuthal mode numbers of involved modes to differ by r . This corresponds to the first peak in $\text{Im } x$. In the next (third) order perturbation theory we expect that Fourier harmonics

$$\mathcal{F}_{2,pm} = \frac{\varepsilon_p}{8} (\delta_{m-p,\pm 2r} + \delta_{m+p,2r} + 2\delta_{m,p}) \quad (30)$$

with different p and m enter which describe the coupling of modes whose mode numbers differ by $2r$. Hence, we expect that every higher-order perturbation theory reproduces one further peak in $\text{Im } x$.

IV. CONCLUSION AND OUTLOOK

In this paper we studied the reduction of the lifetime of optical modes in deformed microcavities due to resonance-assisted tunneling. We predicted the imaginary part of the complex wave numbers $x = kR$ by modeling one dominant resonance chain in phase space with a generalized pendulum approximation. This allows us to expand the mode of a deformed cavity in modes of a circular cavity and deduce

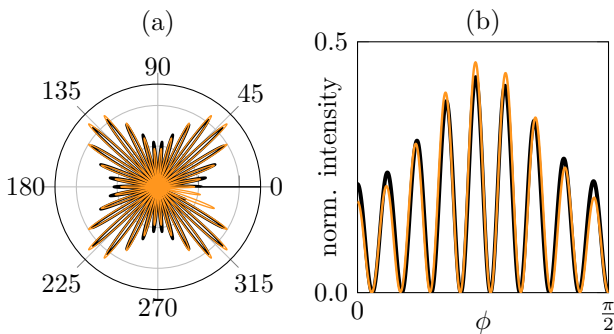


FIG. 6. The far-field intensity pattern of the mode $(m, l) = (21, 1)$ in system \mathcal{A} is shown (a) in a polar plot and (b) for the symmetry reduced part of the radiation angle ϕ . The light orange curve corresponds to the RAT prediction while the black curve represents numerical calculation (BEM). Both far-field intensities are normalized to the area below the curve in (b).

the couplings by perturbation theory of resonance-assisted tunneling. Additionally, the dielectric boundary conditions are crucial for optical microcavities. Therefore, we incorporate an effective shift in the momentum of the optical modes when we compare them to the classical phase space. Furthermore, we predicted the internal and far-field mode structure in the deformed cavity. We studied three systems where we change either the order of the dominant resonance chain or the perturbation strength, which shows the validity of our method up to systems with a mixed phase space and large chaotic layer around the resonance chain. However, we analyze tunneling through one resonance chain in the phase space. For higher

values of $Re\,x$ or strong boundary deformations, multiple resonance chains become important and need to be included in the prediction similar to case of maps [20].

Our results motivate the extension of perturbation theory for weakly deformed optical microcavities derived by Dubertrand *et al.* [26] to third (and higher) orders.

ACKNOWLEDGMENTS

We thank Normann Mertig for fruitful discussions. Financial support from DFG (Project No. WI 1986/7-1) is acknowledged.

-
- [1] L. Markus and K. Meyer, *Generic Hamiltonian Dynamical Systems are Neither Integrable nor Ergodic*, American Mathematical Society: Memoirs of the American Mathematical Society No. 144 (American Mathematical Society, Providence, RI, 1974).
- [2] A. Lichtenberg and M. A. Lieberman, *Regular and Chaotic Dynamics* (Springer, New York, 1992).
- [3] H. Poincaré, *Rend. Circ. Mat. Palermo (1884-1940)* **33**, 375 (2008).
- [4] G. D. Birkhoff, *Trans. Am. Math. Soc.* **14**, 14 (1913).
- [5] M. J. Davis and E. J. Heller, *J. Chem. Phys.* **75**, 246 (1981).
- [6] S. Keshavamurthy and P. Schlagheck, *Dynamical Tunneling: Theory and Experiment* (Taylor & Francis, London, 2011).
- [7] G. Hackenbroich and J. U. Nöckel, *Europhys. Lett.* **39**, 371 (1997).
- [8] A. Bäcker, R. Ketzmerick, S. Löck, J. Wiersig, and M. Hentschel, *Phys. Rev. A* **79**, 063804 (2009).
- [9] J. Jackson, *Classical Electrodynamics* (Wiley, New York, 1975).
- [10] J. Yang, S.-B. Lee, S. Moon, S.-Y. Lee, S. W. Kim, Truong Thi Anh Dao, J.-H. Lee, and K. An, *Phys. Rev. Lett.* **104**, 243601 (2010).
- [11] S.-B. Lee, J. Yang, S. Moon, J.-H. Lee, K. An, J.-B. Shim, H.-W. Lee, and S. W. Kim, *Appl. Phys. Lett.* **90**, 041106 (2007).
- [12] Y.-F. Xiao, X.-F. Jiang, Q.-F. Yang, L. Wang, K. Shi, Y. Li, and Q. Gong, *Laser Photon. Rev.* **7**, L51 (2013).
- [13] V. A. Podolskiy and E. E. Narimanov, *Opt. Lett.* **30**, 474 (2005).
- [14] S. Shinohara, T. Harayama, T. Fukushima, M. Hentschel, T. Sasaki, and E. E. Narimanov, *Phys. Rev. Lett.* **104**, 163902 (2010).
- [15] S. Shinohara, T. Harayama, T. Fukushima, M. Hentschel, S. Sunada, and E. E. Narimanov, *Phys. Rev. A* **83**, 053837 (2011).
- [16] J. U. Nöckel, A. D. Stone, and R. K. Chang, *Opt. Lett.* **19**, 1693 (1994).
- [17] H.-H. Yu, C.-H. Yi, and C.-M. Kim, *Opt. Express* **23**, 11054 (2015).
- [18] O. Brodier, P. Schlagheck, and D. Ullmo, *Ann. Phys.* **300**, 88 (2002).
- [19] O. Brodier, P. Schlagheck, and D. Ullmo, *Phys. Rev. Lett.* **87**, 064101 (2001).
- [20] S. Löck, A. Bäcker, R. Ketzmerick, and P. Schlagheck, *Phys. Rev. Lett.* **104**, 114101 (2010).
- [21] C. Eltschka and P. Schlagheck, *Phys. Rev. Lett.* **94**, 014101 (2005).
- [22] M. Sheinman, S. Fishman, I. Guarneri, and L. Rebuzzini, *Phys. Rev. A* **73**, 052110 (2006).
- [23] N. Mertig, J. Kullig, C. Löbner, A. Bäcker, and R. Ketzmerick, [arXiv:1607.06477](https://arxiv.org/abs/1607.06477).
- [24] S. Gehler, S. Löck, S. Shinohara, A. Bäcker, R. Ketzmerick, U. Kuhl, and H.-J. Stöckmann, *Phys. Rev. Lett.* **115**, 104101 (2015).
- [25] H. Kwak, Y. Shin, S. Moon, S.-B. Lee, J. Yang, and K. An, *Sci. Rep.* **5**, 9010 (2015).
- [26] R. Dubertrand, E. Bogomolny, N. Djellali, M. Lebental, and C. Schmit, *Phys. Rev. A* **77**, 013804 (2008).
- [27] H. Cao and J. Wiersig, *Rev. Mod. Phys.* **87**, 61 (2015).
- [28] S. Qiu, J. Cai, Y. Li, and Z. Han, *Opt. Commun.* **277**, 406 (2007).
- [29] S. V. Boriskina, T. M. Benson, P. D. Sewell, and A. I. Nosich, *IEEE J. Sel. Top. Quantum Electron.* **12**, 1175 (2006).
- [30] S. C. Creagh and M. M. White, *Phys. Rev. E* **85**, 015201 (2012).
- [31] J. U. Nöckel, Resonances in Nonintegrable Open Systems, Ph.D. thesis, Yale University, 1997.
- [32] J. Wiersig, *J. Opt. A: Pure Appl. Opt.* **5**, 53 (2003).
- [33] M. Kraft and J. Wiersig, *Phys. Rev. A* **89**, 023819 (2014).
- [34] J. Wiersig, *Phys. Rev. A* **85**, 063838 (2012).
- [35] L. Ge, Q. Song, B. Redding, and H. Cao, *Phys. Rev. A* **87**, 023833 (2013).
- [36] L. Ge, Q. Song, B. Redding, A. Eberspächer, J. Wiersig, and H. Cao, *Phys. Rev. A* **88**, 043801 (2013).
- [37] M. Hentschel, H. Schomerus, and R. Schubert, *Europhys. Lett.* **62**, 636 (2003).
- [38] F. Goos and H. Hänchen, *Ann. Phys.* **436**, 333 (1947).
- [39] K. Artmann, *Ann. Phys.* **437**, 87 (1948).
- [40] J. Unterhinninghofen and J. Wiersig, *Phys. Rev. E* **82**, 026202 (2010).
- [41] H. E. Tureci and A. D. Stone, *Opt. Lett.* **27**, 7 (2002).
- [42] H. Schomerus and M. Hentschel, *Phys. Rev. Lett.* **96**, 243903 (2006).
- [43] J. Kullig, C. Löbner, N. Mertig, A. Bäcker, and R. Ketzmerick, *Phys. Rev. E* **90**, 052906 (2014).
- [44] D. A. Wisniacki, M. Saraceno, F. J. Arranz, R. M. Benito, and F. Borondo, *Phys. Rev. E* **84**, 026206 (2011).
- [45] D. A. Wisniacki and P. Schlagheck, *Phys. Rev. E* **92**, 062923 (2015).
- [46] J. Unterhinninghofen, J. Wiersig, and M. Hentschel, *Phys. Rev. E* **78**, 016201 (2008).